LIFT RESPONSE OF A FINITE WINGSAIL TO BOUNDARY LAYER TURBULENCE.

Clement BOUHOURD
CNRS LHEEA UMR 6598
Ecole Centrale Nantes
1 Rue de la Noë, 44300 Nantes, France
clement.bouhourd@ec-nantes.fr

Laurent PERRET
CNRS LHEEA UMR 6598
Ecole Centrale Nantes
1 Rue de la Noë, 44300 Nantes, France
laurent.perret@ec-nantes.fr

Carlo COSSU
CNRS LHEEA UMR 6598
Ecole Centrale Nantes
1 Rue de la Noë, 44300 Nantes, France
carlo.cossu@ec-nantes.fr

ABSTRACT

This study investigates the instantaneous lift response of a rectangular finite wing with a NACA 0012 airfoil, immersed in a high Reynolds number turbulent boundary layer, through wind tunnel experiments. Unsteady aerodynamic forces are measured at the root of the wall-mounted wing, synchronously with the three fluctuating velocity components of the upstream flow at the wing tip. The primary objective of this study is to elucidate the contribution to the unsteady wing lift of the three velocity components, their associated squared value and the cross-component terms for three different angles of attack. A multi-input / single-output model is derived using spectral methods to attribute the respective contributions. This study demonstrates a high level of coherence between the measured oncoming velocity fluctuations and the lift force fluctuations, with 30% of the lift variance correlated to the incoming turbulence. Additionally, we show that cross-component terms are strongly correlated with lift fluctuations at small angles of attack. As the angle of attack increases, the linear terms become the dominant contributors to lift fluctuations with streamwise fluctuations in the low wavenumber range, and the transverse component in the energy-containing range.

INTRODUCTION

The challenge of reducing the global CO_2 emissions has renewed the interest in wind-assisted propulsion for cargo ships. To this end, different technologies are considered for their potential gains in performance such as kites, Flettner rotors, suction sails and rigid wingsails. This work focuses specifically on wingsails. These lifting surfaces operate in the lower part of the atmospheric boundary layer where turbulence can significantly impact the aerodynamic performance of the systems. In such real-world environments, the aerodynamic forces are highly unsteady, leading to undesirable vibrations and noise. Predicting the force fluctuations is therefore critical for sizing the mechanical structures and prevent them from fatigue and premature breakage.

Understanding and predicting the link between the turbulence and the fluctuating aerodynamic forces has been a point of interest for decades. Building on thin-airfoil theory, Sears (1941) derived the lift response of a two-dimensional airfoil at zero angle of attack (AoA) to a sinusoidal gust normal to the chord. In the Sears function, the lift response of the wing strip is directly related to the one-wavenumber gust normal to the wing planform, assuming perfect spanwise coherence of the wind. Liepmann (1952) extended the discrete frequency approach of Sears to continuous spectrum, paving the way for the relationship between aerodynamic force fluctuations and turbulence spectra, a concept now known as aerodynamic admittance. To account for the three-dimensionality of turbulence, Graham (1970) introduced a two-wavenumber transfer function and derived its exact solution using lifting-surface theory for an airfoil of infinite span length at zero AoA and zero-thickness. The Graham function was later experimentally validated by Jackson et al. (1973) and Li et al. (2015). Goldstein & Atassi (1976) added the contribution of the streamwise component to the Sears function and Atassi (1984) corrected the lift formula to take into account the influence of the AoA, the airfoil camber and the thickness.

In recent experiments, Li et al. (2018, 2022) and Zhao et al. (2025) introduced a method to measure the one-wavenumber aerodynamic admittance on an airfoil subjected to grid turbulence. This method validated and revealed the robustness of the originale theoretical works made by Sears (1941), Graham (1970) and Atassi (1984) across a range of conditions, including varying the integral length scale of the oncoming turbulence, aspect ratio and angle of attack.

In the marine environment, wingsails operate under flow conditions that differ significantly from those studied in aerodynamic wind tunnels. Specifically, wingsails

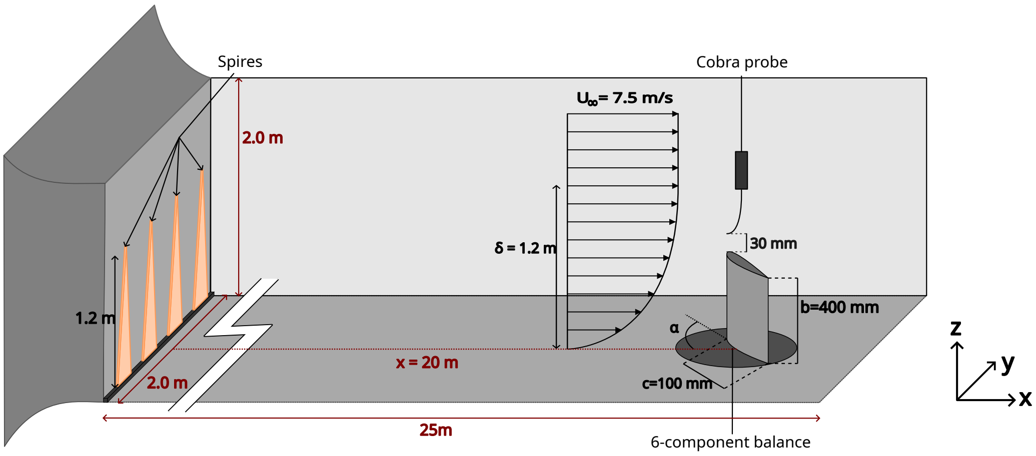

Figure 1. Experimental setup.

Table 1. Characteristic quantities of the present study.

U_∞	U_τ	z_0	δ	Re_τ	b/δ	c/δ	Re_c
7.5 m/s	0.56 m/s	17 µm	1.2 m	40 000	0.35	0.087	38 000

perform within the atmospheric surface layer (ASL), where the oncoming wind is highly inhomogeneous and anisotropic. In such wall-bounded flows, investigation-sprevious studies highlighted the co-habitation of different organized turbulent motions (Smits et al., 2011). Elongated low-streamwise-momentum region in the inner layer, also called large-scale motions (LSMs) (Adrian et al., 2000) and superstructures (Hutchins & Marusic, 2007) present in the surface layer could influence the lift response of wingsails. Additionally, the characteristic energy-containing turbulence length scales in the hundreds of meters are substantially larger than the chord lengths ($c \approx 10$ m) of these lifting bodies.

Throughout this paper, u, v and w will be used to denote the velocity components in the streamwise x, the transverse y and wall-normal z directions, respectively. In the previous cited experimental works, the lift force is linearly linked to turbulence terms and especially the transverse wind component v normal to the wing planform. However, in a turbulent boundary layer, anisotropy and inhomogeneity could yield to non-negligible contribution of higher order turbulence terms to lift fluctuations. As a first approximation, for small AoA ($\alpha << 1$ rad), the lift force on a two-dimensional strip can be expressed as

$$l_{2D}(z,t) = 2\pi\alpha(z,t)\rho c|\mathbf{u}(z,t)|^2, \quad (1)$$

where ρ is the fluid density, c the chord length of the airfoil, $\mathbf{u} = (u, v)$ is the incident velocity vector and α is the AoA of the wing. The linearization of eq. (1) around the steady state (α_0, U_0) yields the following expression for the lift perturbation

$$\frac{l'_{2D}}{2\pi\rho c U_0^2} \simeq \alpha_0(2u'/U_0 + u'^2/U_0^2 + v'^2/U_0^2) + (v'/U_0 + v'u'/U_0^2), \quad (2)$$

where only first and second order terms were maintained. Although this expression does not account for the two-wavenumber transfer function derived by Graham (1970), it highlights the potential contribution of higher-order turbulence terms to aerodynamic force fluctuations.

This work aims to quantify the contribution of up to the second-order turbulence terms on a finite rectangular wing immersed in a turbulent boundary layer, focusing on three angles of attack: $\alpha_0 = 0°$, $5°$ and $14°$. To achieve this, synchronous measurements of both the global aerodynamic forces and the upstream turbulent velocity are performed to enable the derivation of a Multi-Input / Single Output (MISO) model using spectral methods as proposed by Bendat (1998) and Bendat & Piersol (2010).

METHODS
Experimental details

The experiments have been performed in the atmospheric wind tunnel of the Laboratoire de recherche en hydrodynamique, énergetique et environnement atmospherique (LHEEA) at Ecole Centrale Nantes (figure 1). The wind tunnel is a 25-meter-long open-circuit facility with a 2 m×2 m cross-section. The oncoming flow is a turbulent boundary layer, generated using four 1.2-meter-high tapered spires installed downstream of the convergent. The boundary layer is further developed with perforated metal plates (diameter = 5 mm, depth = 2 mm) on the wind tunnel floor. The freestream wind speed (U_∞) is 7.5 m/s. This configuration mimics a scaled neutral marine atmospheric boundary layer (Schliffke, 2022) whose Reynolds number is $Re_\delta = U_\tau\delta/\nu = 40000$ at the position of the test section ensuring scale separation between the inner and the outer layers and fully developed turbulent structures as detailed in Smits et al. (2011), where U_τ is the skin friction velocity, δ the boundary-layer thickness and ν the kinematic viscosity of air. All the relevant quantities associated to the oncoming turbulent boundary

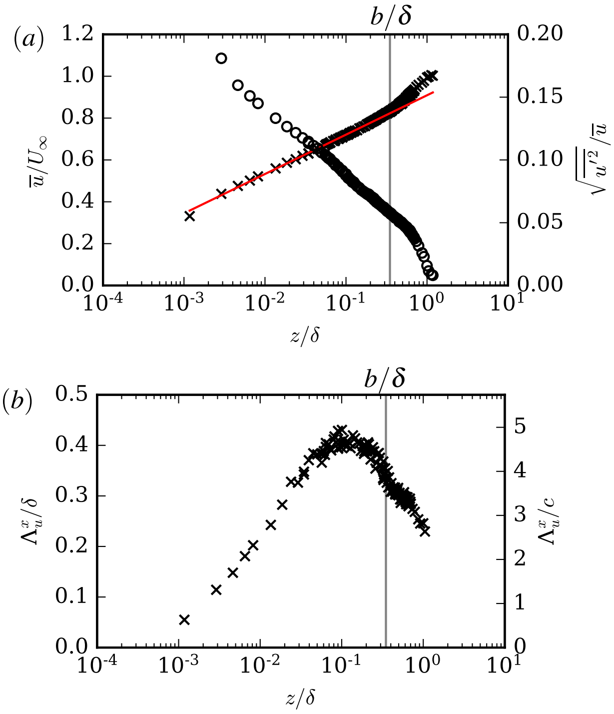

Figure 2. Wall-normal evolution of (a) the mean $(\overline{u})$ and the turbulence intensity $(\sqrt{\overline{u'^2}}/\overline{u})$ of the streamwise velocity component within the turbulent boundary layer and (b) the streamwise longitudinal integral length scale at the location of the finite wing. In (a), the red solid line represents the theoretical log-law expressed as $\overline{u}(z) = (U_\tau/\kappa)\ln(z/z_0)$, where U_τ is the skin friction velocity, $\kappa = 0.4$ the Von Kàrmàn constant, z_0 the aerodynamic roughness length. U_∞ is the freestream velocity and δ the 99% boundary-layer thickness. The grey vertical line indicates the extent of the wing within the boundary layer.

layer are detailed in table 1. Flow characteristics in the wind tunnel were measured using hot-wire anemometry. Theory predicts a logarithmic dependence of the mean longitudinal wind component to the wall-normal distance (Pope, 2000). This theoretical prediction agrees with the experimental data shown in figure 2.a up to $z/\delta \approx 0.4$. The wall-normal distribution of the longitudinal turbulence intensity and the streamwise integral length scale of the longitudinal velocity component of the oncoming turbulence are displayed in figure 2. Under the present flow conditions, the energy-containing turbulence scales are significantly larger than the chord length of the wing which is a notable aspect of this study.

In this study, a rectangular finite wing was vertically mounted on a 6-component balance (ATI Gamma Force/Torque Sensor) located under the wind tunnel floor to measure the unsteady aerodynamic forces. The wing has a span of $b = 400$ mm and a chord length of $c = 100$ mm with a cross-section based on a NACA 0012 airfoil. To minimize fluid-structure interactions in the collected force data due to wing vibrations, the core of the model is made with extruded polystyrene with unidirectional high-modulus carbon fibers spars inserted at the maximum thickness of the wing. The core is enveloped with $+45°$, $-45°$ carbon fiber sheets. This choice guarantees an optimal stiffness-to-density ratio of the model, resulting in a natural frequency of the wing of $f_R = 60$ Hz. The blockage ratio associated to the finite wing is less than 1%. The wing is fully immersed in the log-law region of the oncoming flow. The instantaneous velocity at the wing tip is measured using a TFI Cobra Probe positioned 30 mm above the wing tip. The Cobra Probe is a four-hole pressure-based probe able to resolve the 3 components of the velocity with an uncertainty of ± 0.3 m.s^{-1} and a maximum sampling frequency of 1.2 kHz. The data acquisition system recorded measurements at a sampling frequency of 5 kHz, with a total acquisition duration of 28 800 s= $1.8 \cdot 10^5 \delta/U_\infty$. The reference velocity is defined as the mean longitudinal wind value integrated along the wingspan ($U_0 = \frac{1}{b}\int_0^b U(z)dz$), giving a chord-based Reynolds number of $Re_c = U_0 c/\nu = 38\,000$.

Multi-Input/Single-Output System

To analyze the contribution of the three velocity components and the characteristics of the link velocity-forces, MISO models are derived using spectral transfer functions, for several angles of attack. Using the Reynolds decomposition, any quantity is written as $y(t) = Y + y'(t)$ where $Y = \overline{y}$ is the arithmetic mean and y' its fluctuating part. In this work, the MISO model takes the fluctuations of the three linear velocity fluctuations (u', v', w'), squared velocity fluctuations (u'^2, v'^2, w'^2) and cross-component velocity fluctuations ($u'v'$, $u'w'$, $v'w'$) as inputs. The output is the lift force fluctuations (l') acting on the finite wing. The set of inputs will be denoted by I. When correlation exists between any pair of input records (e.g e_i and e_j), the contribution from the input e_j to the output can be partially or entirely attributable to another input e_i. To eliminate this potential bias, the inputs must be conditioned by removing any linear contribution of e_r in e_j for $r < j$. In this study, all inputs are conditioned. For simplicity, they will continue to be denoted by their original, non-conditioned symbols. The contributions from the different inputs are estimated using the partial coherence function defined by Bendat & Piersol (2010) as

$$\gamma_{il}^2(k_1) = \frac{|\phi_{il}(k_1)|^2}{\phi_{ii}(k_1)\phi_{ll}(k_1)}, \quad \text{for} \quad i \in I \tag{3}$$

where the subscript 'l' denotes the lift force signal, ϕ_{il} cross-spectrum density between the quantity e_i and the lift, and, ϕ_{ll} & ϕ_{ii} are power spectral densities. The multiple coherence function is defined as

$$\gamma_{Jl}^2 = \sum_i^J \gamma_{il}^2, \quad \text{for} \quad J \subseteq I. \tag{4}$$

For $J = I$, the multiple coherence then becomes the total coherence function, denoted by $\gamma_l{}^2$ which assigns the total contribution of the turbulence to the lift fluctuations. This function has one as least upper bound : for a perfectly linear system, fully described by the inputs, the multiple coherence function should be unity (Bendat & Piersol, 2010).

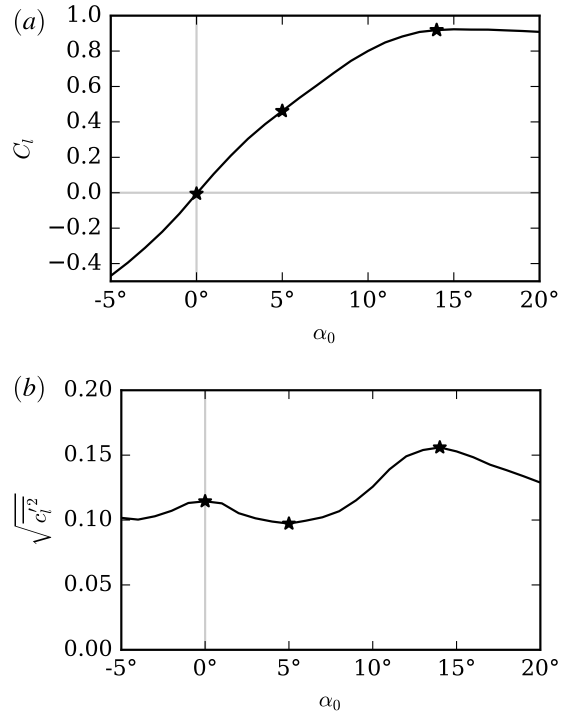

Figure 3. (*a*) Mean and (*b*) root mean square of the lift coefficient versus the angle of attack in the turbulent boundary layer. Markers highlight the three selected angles of attack of the present study.

RESULTS

The time-average and root mean square (rms) of the lift coefficient on the finite wing are presented in figure 3 versus the AoA measured in the turbulent boundary layer. The three selected AoAs $\alpha_0 = 0°$, 5° and 14° are illustrated with markers. These angles were chosen to represent distinct aerodynamic regimes: zero lift, linear lift dependence on α, and high-lift conditions, respectively. The non-linear dependence of the lift coefficient on α_0 is attributed to well-documented low-Reynolds-number effects (Winslow et al., 2018), though these effects are not discussed further in the present study.

The premultiplied one-wavenumber power spectral densities (PSDs) of both the unconditioned and conditioned inputs, measured at the wing tip, are presented in figure 4. The inputs are categorized into three distinct subsets containing the linear terms (I_1), the squared terms (I_2) and the cross-component terms (I_3), respectively. Results are shown for an arbitrary α_0 as the measured inflow spectra are independent of this parameter. Figure 4 indicates that the decorrelation process has an influence on certain inputs, such as the w', $u'w'$ and $v'w'$. This influence arises due to surface-layer turbulent structures, where the following correlations are non-zero: $\overline{u'w'} \neq 0$, $\overline{u'w'^2} \neq 0$ and $\overline{w'v'^2} \neq 0$. However, the effects of the decorrelation process remain negligible for the other inputs.

The premultiplied one-wavenumber PSDs of the fluctuating lift force are presented with full lines in figure 5.a for $\alpha_0 = 0°$, 5° and 14°. For small AoA, the energy-containing fluctuations of the lift force aligns with the energy-containing length scale of turbulence. As the AoA increases up to the stall condition the lift force spectrum shifts to higher frequency. The Strouhal number, calculated at the reduced frequency where the premultiplied PSD reaches its maximum for $\alpha_0 = 14°$, is $St = f \times c\sin(\alpha_0)/U_0 = 0.19$. This suggests that the lift PSD shifts toward frequencies associated with vortex shedding. The fraction of the lift spectrum correlated with the inputs is shown with dashed lines in figure 5.a. 30% of the variance of the lift is correlated to the inputs measured at the wing tip, independently of the AoA. In the present study, the turbulence-lift correlation does not reach 100%. The primary explanation is that the transfer function is build from a one-point turbulent measurement with the total lift acting on the wing. With only one-point measurement, the three-dimensionality of the turbulence cannot be taken into account and reduces considerably the turbulence-lift correlation (Ma et al., 2019).

The figure 5.b presents the total coherence functions between the inputs I and the lift fluctuations for the three different AoAs. This figure reveals that the level and the frequency range of the turbulence-lift correlation remains almost unchanged when varying α_0. For the different AoAs, the total coherence is close to unity ($0.6 > \gamma_l > 0.3$) for reduced frequencies up to 0.1 then drops to zero with the same slope for the different AoAs. The evolution of the coherence function is consistent with the three-dimensional turbulence correction proposed by Li et al. (2018).

The MISO model gives access to spectral contributions from the different inputs to the lift fluctuations. The figure 6 presents the partial contribution of the inputs split into the three distinct subsets presented earlier. The total contribution of the inputs I to the lift fluctuations is represented by the shaded area on each graph. It is interesting to notice that the fluctuations of the streamwise components do not contribute to the lift fluctuations for $\alpha_0 = 0°$ as expected by eq. (2) and derived by Atassi (1984). When increasing α_0, u' begins to contribute and becomes predominant at low reduced frequencies while v' remains the main contributor in the energy-containing range. At small AoA, the $u'v'$ term is the predominant non-linear term. Its importance decreases as the AoA increases and becomes negligible close to stall conditions. The presence of a non-negligible contribution of u' and $u'v'$ may be the footprint of interactions between the elongated streaky structures present in the boundary layer and the lift response at low wavenumber. The $v'w'$ term also arises at small AoA. Its origin may be attributed to three-dimensional effects. This point remains to be further investigated. The black dashed lines in figure 6 show the multiple coherence function of each set of inputs. The area between the multiple coherence function and the total coherence function for the I_1 subset represents the contribution neglected when the linear terms are the only considered inputs. This area is not negligible for α_0 but reduces drastically when increasing α_0 and is almost null at $\alpha = 14°$. This suggests that linear terms that must include both u' and v' are sufficient to describe the lift fluctuations when the time-averaged lift force is non-zero.

CONCLUSION

The main goal of this study was to use a Multi-Input/Single-Output (MISO) modeling approach to relate the contribution of the turbulence to the aerody-

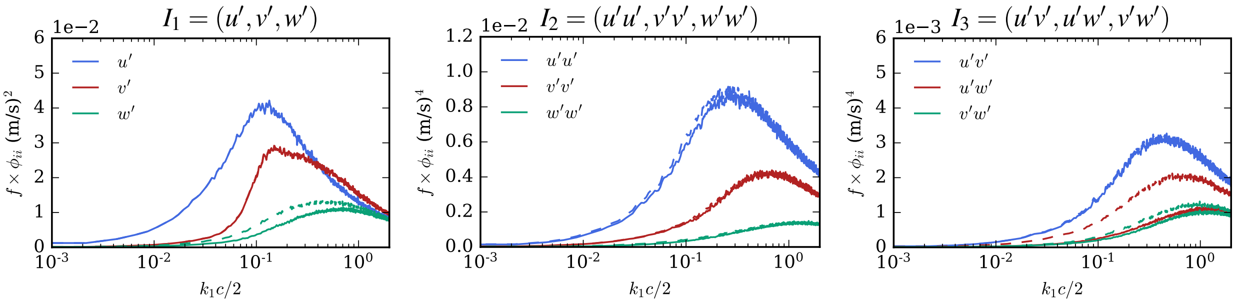

Figure 4. Premultiplied power spectral density of unconditioned (dashed lines) and conditioned (full lines) inputs separated in three subsets $I_1 = (u', v', w')$, $I_2 = (u'u', v'v', w'w')$ and $I_3 = (u'v', u'w', v'w')$. Scales and units of the y-axis vary with graphs.

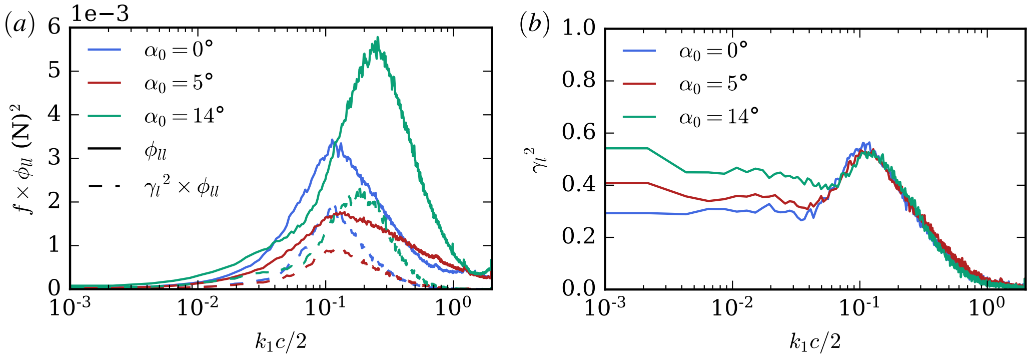

Figure 5. (a) Premultiplied PSD of lift for the different angles of attack, and (b) total coherence function between the inputs I and the lift fluctuations. In (a), the full lines represent the lift PSD based on force measurements, while dashed lines correspond the portion lift PSD correlated to inputs I.

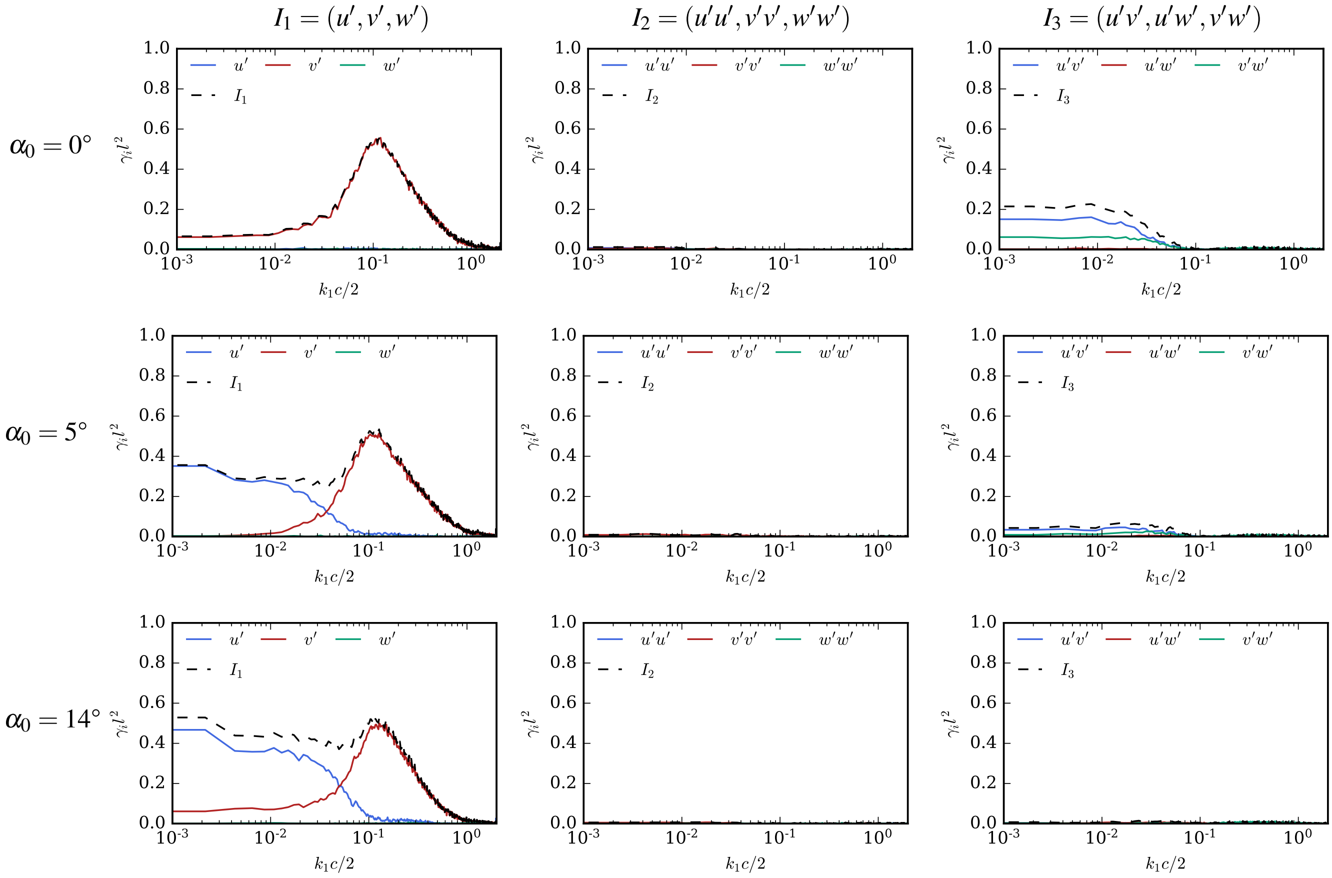

Figure 6. Partial coherence functions for $\alpha_0 = 0°$ (top row graphs), $5°$ (middle row graphs) and $14°$ (bottom row graphs). The contributions from the different subsets are presented in column, with $I_1 = (u', v', w')$ (left column), $I_2 = (u'u', v'v', w'w')$ (middle column) and $I_3 = (u'v', u'w', v'w')$ (right column). The grey surfaces show the total coherence functions for the associated AoA. The black dashed lines shows the multiple coherence functions associated to each subset of inputs.

namic force fluctuations. This method was applied to a finite rectangular wing immersed in a high Reynolds number turbulent boundary layer, using synchronous measurements of the inflow three velocity components at the wing tip and the total lift force at the wing root. The inputs of the MISO model were organized in three subsets which contain the linear turbulence terms (u', v', w'), the squared turbulence terms $(u'u', v'v', w'w')$ and the cross-component turbulence terms $(u'v', u'w', v'w')$. The contribution of these inputs were compared to the aerodynamic lift force fluctuations acting on the finite wing was analysed for three angles of attack: $\alpha_0 = 0°$, 5° and 14°.

The main novelty of this study lies in the inflow conditions. The finite wing was fully immersed in the logarithmic layer of high Reynolds number turbulent boundary layer, where anisotropy and inhomogeneity are most pronounced, and where energy-containing turbulence structures are larger than the characteristic length scales of the wing. Under theses conditions, the contribution of non-linear turbulence terms on the lift fluctuations was investigated.

This study demonstrates a high level of correlation between the turbulence measured at the tip of the wing and the total lift fluctuations, accounting for 30% of the total lift variance, independent of the angle of attack. At zero angle of attack, $u'v'$ and v' are primary drivers of the lift fluctuations, with no contribution from u'. As the angle of attack increases, u' and v' become prominent contributors. The terms $u'v'$ and u' have a non-negligible contribution to lift fluctuations in the low wavenumber range. These contributions may be attributed to the large-scale and very large-scale motions present in the logarithmic region of the oncoming boundary layer. In the energy-containing range, v' has a well-known contribution for all the considered angles of attack.

Future work will be conducted in turbulent boundary layer to take into consideration the finite coherence length of the turbulence along the wingspan as well as the spatial inhomogeneity of the turbulent boundary layer flows.

REFERENCES

Adrian, R. J., Meinhart, C. D. & Tomkins, C. D. 2000 Vortex organization in the outer region of the turbulent boundary layer. Journal of Fluid Mechanics 422, 1–54.

Atassi, H. M. 1984 The sears problem for a lifting airfoil revisited - new results. Journal of Fluid Mechanics 141, 109–122.

Bendat, J. S. 1998 Nonlinear systems techniques and applications. Wiley.

Bendat, J. S. & Piersol, A. G. 2010 Random data: analysis and measurement procedures, 4th edn. Wiley.

Goldstein, M. E. & Atassi, H. 1976 A complete second-order theory for the unsteady flow about an airfoil due to a periodic gust. Journal of Fluid Mechanics 74, 741–765.

Graham, J. M. R. 1970 Lifting surface theory for the problem of an arbitrarily yawed sinusoidal gust incident on a thin aerofoil in incompressible flow. Aeronautical Quarterly 21, 182–198.

Hutchins, N. & Marusic, Ivan 2007 Evidence of very long meandering features in the logarithmic region of turbulent boundary layers. Journal of Fluid Mechanics 579, 1–28.

Jackson, R., Graham, J. M. R. & Maull, D. J. 1973 The lift on a wing in a turbulent flow. Aeronautical Quarterly .

Li, M., Yang, Y., Li, M. & Liao, H. 2018 Direct measurement of the sears function in turbulent flow. Journal of Fluid Mechanics 847, 768–785.

Li, M., Zhao, Y., Yang, Y. & Zhou, Q. 2022 Aerodynamic lift fluctuations of an airfoil in various turbulent flows. Journal of Fluid Mechanics 947, A21.

Li, S., Li, M. & Liao, H. 2015 The lift on an aerofoil in grid-generated turbulence. Journal of Fluid Mechanics 771, 16–35.

Liepmann, H. W. 1952 On the application of statistical concepts to the buffeting problem. Journal of the Aeronautical Sciences 19, 793–800.

Ma, C., Wang, J., Li, Q. S. & Liao, H. 2019 3D aerodynamic admittances of streamlined box bridge decks. Engineering Structures 179, 321–331.

Pope, S. B. 2000 Turbulent flows. Cambridge: Cambridge Univ. Press.

Schliffke, B. 2022 Experimental characterisation of the far wake of a modelled floating wind turbine as a function of incoming swell. PhD Centrale Nantes .

Sears, W. R. 1941 Some aspects of non-stationary airfoil theory and its practical application. Journal of the Aeronautical Sciences 8 (3), 104–108.

Smits, A. J., McKeon, B. J. & Marusic, I. 2011 High–reynolds number wall turbulence. Annual Review of Fluid Mechanics 43 (1), 353–375.

Winslow, J., Otsuka, H., Govindarajan, B. & Chopra, I. 2018 Basic understanding of airfoil characteristics at low reynolds numbers (104–105). Journal of Aircraft 55 (3), 1050–1061.

Zhao, Y., Yang, Y. & Li, M. 2025 The lift on an airfoil at various angles of attack in turbulent flow. Journal of Fluid Mechanics 1010, A45.